

Interaction-induced edge states in HgTe/CdTe quantum wells under a magnetic field

Zewei Chen and Tai Kai Ng*

Physics Department, The Hong Kong University of Science and Technology, Hong Kong



(Received 30 June 2018; revised manuscript received 28 May 2019; published 28 June 2019)

In this paper, we study doped HgTe/CdTe quantum wells with Hubbard-type interaction under a perpendicular magnetic field using a lattice Bernevig-Hughes-Zhang (BHZ) model with a bulk inversion asymmetry (BIA) term. We show that the BIA term is strongly enhanced by interaction around the region when the band inversion of the topological insulator is destroyed by a magnetic field. The enhanced BIA term creates edge-like electronic states which can explain the experimentally discovered edge conductance in doped HgTe/CdTe quantum wells in a similar magnetic field regime.

DOI: [10.1103/PhysRevB.99.235157](https://doi.org/10.1103/PhysRevB.99.235157)

I. INTRODUCTION

Two-dimensional (2D) topological insulators have been extensively studied both theoretically and experimentally since their discovery [1–9]. The nontrivial topology and the helical edge states are protected by time reversal symmetry (TRS) [10]. The detailed behavior of HgTe/CdTe quantum wells under a perpendicular magnetic field has been studied both experimentally [7] and theoretically [11–13]. It is believed that a transition from quantum spin Hall (QSH) state to integer quantum Hall (IQH) state occurs when the magnetic field is strong enough. The Landau level fan charts (LLFC) show a crossing at a critical magnetic field B_c where the band inversion disappears. The helical edge state is destroyed around the transition regime and (chiral) edge states emerge when the system transits into the IQH state. When a bulk inversion asymmetry term is included, the electron and hole bands hybridize and crossing is avoided. These results have been confirmed by magnetospectroscopy studies in HgTe/CdTe quantum wells [14,15].

Edge transport under a perpendicular magnetic field has been studied by Du's group in InAs/GaSb quantum wells [16] in a magnetic field range believed to be below B_c [17]. Shen's group measured the local conductance under a perpendicular magnetic field in doped HgTe/CdTe quantum wells [18] and found that the edge conductance persists under strong magnetic fields up to 9 T, much larger than the expected critical field B_c but still not strong enough to reach the IQH regime; the electron/hole filling factor in the experiment is still too small to fill the zeroth LL. Furthermore, the edge conductance exists only when it is electron-like gated, indicating the importance of particle-hole asymmetry. The noninteracting Bernevig-Hughes-Zhang (BHZ) model is not able to explain these results and suggests that electron interaction may be important to understand the HgTe/CdTe system [18].

In this paper we study the interaction effect in doped HgTe/CdTe quantum wells via a modified lattice BHZ model that takes into account the bulk inversion asymmetry (BIA)

term and with Hubbard-type on-site interaction. The BIA term is found to be small in band structure calculations and is usually neglected. We find that BIA is enhanced by the combined effect of interaction and magnetic field in a self-consistent mean-field theory. The enhanced BIA term gives rise to edge-like states around the region where the band inversion is destroyed by a magnetic field and can explain the experimental results for HgTe/CdTe quantum wells by Shen's group [18].

II. MODEL

We consider the BHZ model with BIA asymmetry term and Hubbard-type on-site interaction on a square lattice with two orbitals $\{|E\sigma\rangle, |H\sigma\rangle\}$ per site. The BIA term is allowed because HgTe/CdTe has a zinc-blende structure which breaks bulk inversion symmetry [6]. We also apply a magnetic field perpendicular to the lattice plane. The system is described by the Hamiltonian $H = H_{\text{BHZ}} + H_{\text{BIA}} + H_z + H_U$, where $H_{\text{BHZ}} = T + H_0$ is the (lattice) BHZ model with

$$H_0 = \sum_{i,\sigma} (\varepsilon_E C_{i,E,\sigma}^\dagger C_{i,E,\sigma} + \varepsilon_H C_{i,H,\sigma}^\dagger C_{i,H,\sigma}), \quad (1a)$$

where ε_τ is the on-site energy for the τ orbital, $C^\dagger(C)_{i,\tau,\sigma}$ creates/annihilates a τ -orbit ($\tau = E, H$) electron with spin $\sigma = \uparrow, \downarrow$ on site i , and

$$T = \sum_{\langle i,j \rangle, \sigma} (t_E C_{i,E,\sigma}^\dagger C_{j,E,\sigma} + t_H C_{i,H,\sigma}^\dagger C_{j,H,\sigma}) \quad (1b)$$

$$+ \sum_{i,\sigma} t_{EH} [s(i C_{i,E,\sigma}^\dagger C_{i+\hat{x},H,\sigma} - i C_{i,E,\sigma}^\dagger C_{i-\hat{x},H,\sigma}) \quad (1c)$$

$$+ (C_{i,E,\sigma}^\dagger C_{i+\hat{y},H,\sigma} - C_{i,E,\sigma}^\dagger C_{i-\hat{y},H,\sigma})] + \text{H.c.} \quad (1d)$$

describes electron hopping between nearest neighbor (NN) lattice sites $\langle i, j \rangle$ where t_τ, t_{EH} denote intraorbital and interorbital hopping, respectively. $s = +(-)1$ for $\sigma = \uparrow (\downarrow)$. H.c. denotes the Hermitian conjugate. The BIA term is

$$H_{\text{BIA}} = -\Delta_0 \sum_i (C_{i,E,\uparrow}^\dagger C_{i,H,\downarrow} - C_{i,H,\uparrow}^\dagger C_{i,E,\downarrow}) + \text{H.c.}, \quad (1e)$$

*phtai@ust.hk

where $\Delta_0 \sim 1.5\text{--}2$ meV, and

$$H_z = \sum_{i,\tau,\sigma} sg_\tau \mu_B B_z C_{i,\tau,\sigma}^\dagger C_{i,\tau,\sigma} \quad (1f)$$

is the Zeeman energy. μ_B is the Bohr magneton and g_τ is the g factor for the τ orbit. B_z is the magnetic field strength. The orbital magnetic field effect is included by Peierls substitution, $t_\tau \rightarrow t_\tau \exp[i2\pi(j-1)\Phi/\Phi_0]$ with gauge field $\mathbf{A} = -B_z y \hat{x}$ (Landau gauge). $\Phi = B_z a^2$ is the magnetic flux passing through a lattice cell and $\Phi_0 = h/e$ is the magnetic flux quantum.

The Hubbard interaction term reads,

$$H_U = \sum_{i;\tau=E,H} U_\tau n_{i,\tau,\uparrow} n_{i,\tau,\downarrow} + \sum_{i;\sigma,\sigma'} U_{EH} n_{i,E,\sigma} n_{i,H,\sigma'}, \quad (2)$$

where U_τ ($\tau = E, H$), $U_{EH} > 0$ describe intra- and interorbital repulsive interactions between electrons, respectively, and $n_{i,\tau,\sigma} = C_{i,\tau,\sigma}^\dagger C_{i,\tau,\sigma}$.

We shall treat the interaction term in a mean-field theory where

$$\begin{aligned} n_{i,\tau,\sigma} n_{i,\tau',\sigma'} & \approx \langle n_{i,\tau,\sigma} \rangle n_{i,\tau',\sigma'} + \langle n_{i,\tau',\sigma'} \rangle n_{i,\tau,\sigma} \\ & - \langle n_{i,\tau,\sigma} \rangle \langle n_{i,\tau',\sigma'} \rangle \\ & - (\langle C_{i,\tau,\sigma}^\dagger C_{i,\tau',\sigma'} \rangle C_{i,\tau,\sigma}^\dagger C_{i,\tau',\sigma'} + \langle C_{i,\tau',\sigma'}^\dagger C_{i,\tau,\sigma} \rangle C_{i,\tau,\sigma}^\dagger C_{i,\tau',\sigma'}) \\ & - \langle C_{i,\tau',\sigma'}^\dagger C_{i,\tau,\sigma} \rangle \langle C_{i,\tau,\sigma}^\dagger C_{i,\tau',\sigma'} \rangle \delta_{\bar{\tau},\tau'} \delta_{\sigma,-\sigma'}, \end{aligned}$$

where $\bar{E}(\bar{H}) = H(E)$ and $\langle \dots \rangle$ denotes ground state expectation value. We note that the on-site hybridization term between the E and H orbitals vanishes because of the opposite parity of the two orbitals. The mean-field Hamiltonian is therefore

$$\begin{aligned} H_{MF} & = H_{\text{BHZ}} + H_{\text{BIA}} + H_z \\ & + \sum_{i,\sigma,\tau} (U_\tau n_{i,\tau,-\sigma} + U_{EH} \langle n_{i,\bar{\tau}} \rangle n_{i,\tau,\sigma} \\ & - U_{EH} (\Delta_1 C_{i,E,\uparrow}^\dagger C_{i,H,\downarrow} - \Delta_2 C_{i,H,\uparrow}^\dagger C_{i,E,\downarrow} + \text{H.c.}), \end{aligned} \quad (3)$$

where $\Delta_{1(2)} = +(-)\langle C_{i,H(E),\downarrow}^\dagger C_{i,E(H),\uparrow} \rangle$ couples the spin-up (hole) orbital to the spin-down hole (electron) orbital, respectively, and $n_{i,\tau} = \sum_\sigma n_{i,\tau,\sigma}$. We note that our mean-field theory allows an interaction-modified BIA term $\Delta_0 \rightarrow \tilde{\Delta}_{1(2)} = \Delta_0 + U_{EH} \Delta_{1(2)}$ and also the possibility of magnetic phases with $\langle n_{i,\tau,\sigma} \rangle \neq \langle n_{i,\tau,-\sigma} \rangle$. The mean-field parameters and phase diagram are determined numerically in our study.

We consider the half-filled BHZ model where the chemical potential is in the gap and the system is a topological insulator. To describe the experimental material [18], we start with the parameters appropriate for a 7.5 nm HgTe/CdTe quantum well with $\varepsilon_E = C + M - 4(B + D)/a^2$, $\varepsilon_H = C - M + 4(B - D)/a^2$, $t_E = (D + B)/a^2$, $t_H = (D - B)/a^2$, and $t_{EH} = A/2a$, where C, M, B, D, A , and $g_{|au|}$ are the parameters in BHZ model determined in Ref. [19] (see Appendix A for details). We note, however, that the band-structure parameters can be changed quite significantly upon doping, which is the case of the doped material HgTe/Hg_{0.3}Cd_{0.7}Te (7.0 nm

HgTe/CdTe quantum well) [1,6] where the sign of D/B is found to be inverted in the doped material, corresponding to changing the light-electron, heavy-hole bands into heavy-electron, light-hole bands [6]. We believe that this is also happening in 7.5 nm material for reasons which will become clear later. Therefore, we choose the parameters in our tight binding model to be $t_E = -0.42$ eV, $t_H = 3.32$ eV, $t_{EH} = 0.275$ eV, $\varepsilon_E = 1.67$ eV, and $\varepsilon_H = -13.27$ eV, corresponding to changing $D \rightarrow -D$ in Ref. [19]. We also set $C = 0$ in our calculation since it can be absorbed in the chemical potential. The lattice constant a is chosen to be 1 nm. The phase diagram and mean-field parameters are studied under a perpendicular magnetic field B_z with these parameters, for various values of U_H , U_E , and U_{EH} . We have performed the calculation at $B_z = 0$ and several values of $B_z \geq 3.5$ T. We note that the magnetic unit cell becomes too large for numerical calculation for $B_z < 3.5$ T.

III. RESULTS

The mean-field parameters are determined self-consistently. We first discuss the mean-field phase diagram in the absence of a magnetic field. We find that the system is in the normal, nonmagnetic state ($\langle n_{i,\tau,\sigma} \rangle = \langle n_{i,\tau,-\sigma} \rangle$) for small U_E , U_H , and U_{EH} . For given U_{EH} and U_E , the system transits from *paramagnetic* phase to *ferromagnetic* phase and then to *antiferromagnetic* phase as U_H increases. The phase diagram can be understood by comparing the model with the single band Hubbard model, whose mean-field phase diagram is well studied. We refer the reader to Appendix B for details.

More interestingly, our mean-field theory allows enhancement of BIA terms $\Delta_0 \rightarrow \tilde{\Delta}_{1(2)} = \Delta_0 + U_{EH} \Delta_{1(2)}$. In the following we shall consider weak interactions where the ground state is nonmagnetic at $B_z = 0$. In this limit U_E has almost no effect due to the small occupation number of the E orbital (see Appendix B). In Fig. 1, we show the calculated values of $\Delta_{1(2)}$ and the corresponding interaction modified BIA term $\tilde{\Delta}_{1(2)}$ for different interaction strengths U_H, U_{EH} with fixed $U_E = 1$ eV at $B_z = 0$. We note that $\Delta_1 = \Delta_2$ in this case due to TRS. We observe that $\Delta_{1(2)}$ exhibits a peak at a critical value of interaction. The peak is driven by the closing and reopening of the bulk gap (i.e., destruction of band inversion)

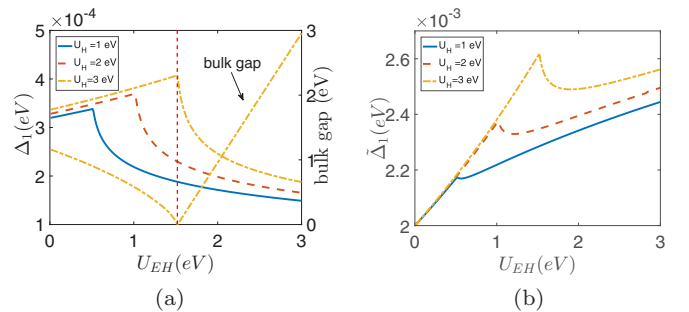


FIG. 1. (a) Self-consistent mean-field results for $\Delta_1 = \Delta_2$ as a function of U_{EH} for several values of U_H at $B_z = 0$ and $U_E = 1$ eV. The left axis represents $\Delta_{1(2)}$ whereas the right axis represents the bulk gap. (b) Interaction modified BIA term $\tilde{\Delta}_1 = \tilde{\Delta}_2$ corresponding to (a).

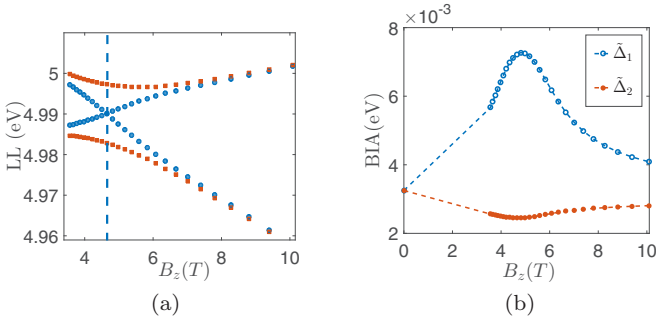


FIG. 2. (a) Lowest LLs as a function of B_z with interaction parameters $U_E = 5$ eV, $U_H = 5$ eV, $U_{EH} = 2.5$ eV. The dots and squares are calculated without and with the BIA term, respectively. The dashed line indicates the position of the critical field. (b) Corresponding $\tilde{\Delta}_{1(2)}$ as a function of B_z .

as a result of change in interaction strengths, suggesting that $\Delta_{1(2)}$ is enhanced by the resonance between the electron and hole energy levels. To see this we also show the bulk gap for $U_H = 3$ eV as a function of U_{EH} in Fig. 1(a). It is clear that the peak position in $\Delta_{1(2)}$ matches with where the bulk gap closes. The interaction modified BIA term $\tilde{\Delta}_1 = \tilde{\Delta}_2$ is plotted in Fig. 1(b). It gets slightly enhanced from Δ_0 , with a maximum enhancement of roughly 30 percent in the band closing region. The small BIA term does not gap out the edge but changes the spin orientation of the helical edge states [6].

Next we study the effect of the magnetic field on the BIA term. We choose the interaction strengths to be $U_E = 5$ eV, $U_H = 5$ eV, and $U_{EH} = 2.5$ eV such that the resulting mean-field band structure at zero magnetic field is almost identical to the one when all interaction strengths are set to be zero [19]. Using these parameters, we study the interaction effect on the BIA term under a perpendicular magnetic field.

In Fig. 2(a) we plot the LL without the BIA term (dots) and with the BIA term (squares). We first consider the LL without the BIA term. In this case the effective Hamiltonian near the Γ point reduces to two decoupled Dirac Hamiltonians at zero magnetic field (see Appendix C). In the presence of a magnetic field, LLs are formed and the zeroth LL wave function contains only one orbital component, E (H) orbital for spin up (down). Due to the band inversion, the zeroth electron-like LL has lower energy than the zeroth hole-like LL at weak magnetic field. As the magnetic field increases, the two zeroth Landau levels (LLs) cross at a critical magnetic field B_c where the band inversion is destroyed. The system transits from a QSH state to an IQH state. The critical magnetic field is found to be around 4.5 T, which is close to the estimation in Ref. [18]. When the BIA term is included, the crossing of the two zeroth LLs is avoided because of hybridization between the two LLs, which is allowed when TRS is broken. In Fig. 2(b) we show the corresponding $\tilde{\Delta}_{1(2)}$ as a function of magnetic field. We note that $\tilde{\Delta}_1 \neq \tilde{\Delta}_2$ in the presence of the magnetic field, and $\tilde{\Delta}_{1(2)}$ shows a peak (dip) at a magnetic field close to the critical magnetic field B_c , suggesting that the peak (dip) in $\tilde{\Delta}_1 \neq \tilde{\Delta}_2$ is driven by resonance between electron and hole energy levels as discussed before. This resonance is absent in trivial band insulators where there is no band inversion. The peak value of the interaction enhanced

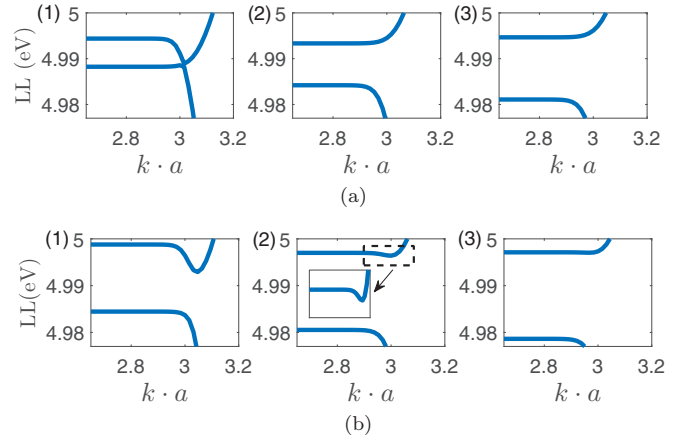


FIG. 3. (a) Band structure for open boundary in y -direction without BIA term at $U_E = 5$ eV, $U_H = 5$ eV, $U_{EH} = 2.5$ eV for different B_z . Columns (1)–(3) are for $B_z = 4, 5.5,$ and 6 T respectively. (b) Band structure with BIA term, with other parameters the same as in (a). The inset in (2) is a zoom-in to show the nontopological edge states.

BIA term $\tilde{\Delta}_1$ is about 3.65 times the bare value Δ_0 . In contrast, $\tilde{\Delta}_2$ is only slightly enhanced, but this enhancement is not important because $\tilde{\Delta}_1$ is the major term responsible for the hybridization between the lowest electron and hole Landau levels.

In the following we study the effect of enhanced $\tilde{\Delta}_1$ under a magnetic field on the edge properties in our model. We consider a sample with periodic boundary in x direction and open boundary in y direction and calculate the corresponding band structure at different magnetic fields $B_z = 4, 5.5, 6$ T, both without and with the BIA term. The result of the calculation as a function of k_x is shown in Fig. 3. We show only the zeroth electron-like and hole-like LLs in Fig. 3, as they contribute to transports in the Shen group's experiment [18]. Without the BIA term [Fig. 3(a)], the edge is gapless when the magnetic field is smaller than the critical field $B_c \sim 4.5$ T. As the magnetic field increases beyond B_c , the two zeroth LLs cross and the system has transited from a QSH state to an IQH state. Edge transport is expected only when the zeroth LL (either electron-like or hole-like) is fully filled.

When the BIA term is added [Fig. 3(b)], a small gap is opened on the edge at $B_z = 4$ T, but edge states with lower energies than the bulk can still be observed by slight gating. At $B_z = 5.5$ T, which is beyond the critical field B_c , we find a small dip near the edge of the zeroth electron-like LL. These (nontopological) edge-like states make possible the unusual edge transports beyond B_c but without IQHE. When the system is gated, electrons have to fill in these edge-like states first before they occupy the bulk LL, making edge conductivity possible. We note that these edge-like states appear only in the zeroth electron-like LL but not in the zeroth hole-like LL, consistent with the experimental result that edge conductivity is observed with positive gate only. Furthermore, we also find that the BIA term decreases when the magnetic field further increases in our calculation. In particular, the nontopological edge-like states disappear and the band structure goes back to that of a normal IQH state when the magnetic field is beyond a

critical value B_e (see calculation result at 6 T), confirming that these edge states are nontopological. We thus predict that the edge transports observed in Shen's experiment will disappear when the magnetic field increases further.

How does a large BIA term create the nontopological edge-like states? To understand the origin of the nontopological edge-like states, we study the quantum Hall problem in a confined system with an effective low energy $\mathbf{k} \cdot \mathbf{p}$ Hamiltonian generated from our mean-field Hamiltonian H_{MF} near $\mathbf{k} = 0$ with the effect of the edge simulated by a confining, linear orbital-dependent potential. The finding of this analysis is summarized in the following. The details of our calculation are given in Appendix C.

In the absence of the hybridization terms $A = 2t_{EH} = \Delta_0 = 0$, the quantum Hall problem reduces to four decoupled LLs described by a harmonic oscillator Hamiltonian with eigenvalues $(n + \frac{1}{2})\omega_\tau$ ($\tau = E, H$), and the linear potential contributes a linear k -dependent shift in energy $\sim \alpha_\tau(k_x l_B^2 - y_0)$ (for $k_x l_B^2 \gg y_0$) to the states near the edge; n = Landau level index and $l_B = \sqrt{\hbar/(e|B_z|)}$ is the magnetic length. The linear potential also shifts the wave function guiding center at the edge by an amount $\Delta y = \xi'_0 l_B$, where $\xi'_0 = 2/\pi$ (see Appendix C). A and Δ_0 introduce hybridization between the LLs, and the Landau level spacing is enhanced by a hybridization gap $\sim |\Delta + cA|$, where $c \sim -\frac{\sqrt{2A\xi'_0}}{2l_B}$ is nonzero only at the edge where the wave function guiding center is shifted by an amount Δy when $\alpha_\tau \neq 0$ (see Appendix C). As a result, the hybridization gap is effectively reduced at the edge. This effect exists only when both A and Δ_0 are nonzero and competes with the linear k -dependent term which tends to increase the energy gap between the electron and hole LLs. When the BIA term is large enough, the later effect dominates in a narrow region of k near the edge. This leads to the appearance of nontopological edge states.

It is interesting to note that the size of region S_τ where these nontopological edges appear in band τ is found to be proportional to the band mass $\sim t_\tau^{-1}$ (see Appendix C). For $D > 0$ ($B < 0$), corresponding to $|t_E| < |t_H|$, we find $S_E > S_H$, consistent with our observation that edge-like states exist only in the electron-like LL [see Fig. 3(b)] and in agreement with Shen's experiment. We note that this conclusion will be inverted if we choose $D < 0$. This is why we expect that the sign of D is inverted in HgTe/Hg_{0.3}Cd_{0.7}Te.

IV. CONCLUSION

Summarizing, we study in this paper the interaction effect in doped HgTe/CdTe quantum wells using a Hubbard-type model. In the weak interaction regime where the system is not magnetically ordered at zero magnetic field, we show that the BIA term is enhanced and exhibits a peak when the system undergoes a band-closing, reopening transition, driven by either interaction or magnetic field. The BIA term is allowed because our system breaks inversion symmetry. The effect is small in zero magnetic field, but the BIA term is enhanced dramatically when the band-closing, reopening transition is driven by a magnetic field, i.e., the QSH to IQH transition. The large BIA term introduces strong hybridization between the zeroth spin-up electron-like LL and the zeroth spin-down

hole-like LL and leads to the formation of edge-like states near the edge which may contribute to edge conductivity in low carrier density when the magnetic field is not too strong. Our result explains the "unexpected" particle-hole asymmetric edge conductivity found in experiment [18] and predicts that the BIA term will decrease again when the magnetic field increases further, leading to vanishing of edge conductivity.

ACKNOWLEDGMENT

We thank HKRGC for support through Grant No. C6026-16W.

APPENDIX A: TIGHT BINDING PARAMETERS

Here we outline how our tight binding Hamiltonian parameters are determined from Ref. [19]. Fourier transforming H_{BHZ} , we obtain

$$H_{BHZ} = \sum_{\mathbf{k}} \Psi_{\mathbf{k}}^\dagger \begin{pmatrix} h(\mathbf{k}) & 0 \\ 0 & h^*(-\mathbf{k}) \end{pmatrix} \Psi_{\mathbf{k}}, \quad (\text{A1})$$

$$h(\mathbf{k}) = \varepsilon_{\mathbf{k}} I_2 + d_\alpha(\mathbf{k}) \cdot \sigma^\alpha,$$

where $\Psi_{\mathbf{k}} = \{C_{E,\mathbf{k},\uparrow}, C_{H,\mathbf{k},\uparrow}, C_{E,\mathbf{k},\downarrow}, C_{H,\mathbf{k},\downarrow}\}^T$, σ^α 's are Pauli matrices,

$$C_{\tau,\mathbf{k},\sigma} = \frac{1}{\sqrt{N}} \sum_i \exp(i\mathbf{k} \cdot \mathbf{R}_i) C_{i,\tau,\sigma}, \quad (\text{A2})$$

where N is the total number of sites, and

$$\begin{aligned} \varepsilon_{\mathbf{k}} &= C - \frac{2D}{a^2} [2 - \cos(k_x) - \cos(k_y)], \\ d_\alpha(\mathbf{k}) &= \left[\frac{A}{a} \sin(k_x), -\frac{A}{a} \sin(k_y), M(\mathbf{k}) \right], \\ M(\mathbf{k}) &= M - \frac{2B}{a^2} [2 - \cos(k_x) - \cos(k_y)], \\ D &= (t_E + t_H)/2, \quad B = (t_E - t_H)/2, \quad A = 2t_{EH}, \\ M &= \frac{\varepsilon_E - \varepsilon_H}{2} - 2(t_E - t_H), \\ C &= \frac{\varepsilon_E + \varepsilon_H}{2} - 2(t_E + t_H). \end{aligned} \quad (\text{A3})$$

Expanding Eq. (A1) around $\mathbf{k} = 0$, we obtained the Hamiltonian (1) in Ref. [19]. All the tight binding parameters and the g_τ factors can be identified from Table I of Ref. [19].

APPENDIX B: MEAN-FIELD PHASE DIAGRAM

We discuss the effect of interaction on HgTe/CdTe quantum wells at zero magnetic field in this Appendix. The mean-field Hamiltonian is

$$\begin{aligned} H_{MF} &= H_{BHZ} + H_{BIA} + H_z \\ &+ \sum_{i,\sigma,\tau} (U_\tau \langle n_{i,\tau,-\sigma} \rangle + U_{EH} \langle n_{i,\bar{\tau}} \rangle) n_{i,\tau,\sigma} \\ &- U_{EH} (\Delta_1 C_{i,E,\uparrow}^\dagger C_{i,H,\downarrow} - \Delta_2 C_{i,H,\uparrow}^\dagger C_{i,E,\downarrow} + \text{H.c.}), \end{aligned} \quad (\text{B1})$$

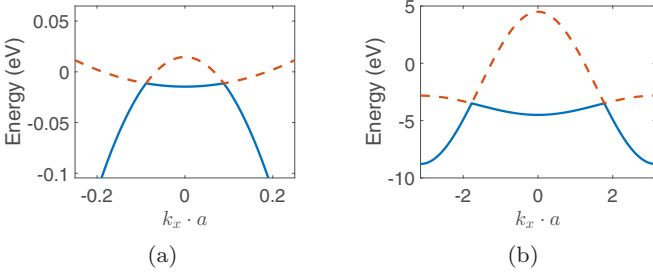


FIG. 4. Schematic band structure illustrating the filling of the E and H bands. The solid/dashed lines denote the parts of bands which are occupied/empty. (a) The case for small band inversion corresponding to HgTe/CdTe quantum wells. (b) The situation with large band inversion.

where $\Delta_{1(2)} = (-)\langle C_{i,H(E),\downarrow(\uparrow)}^\dagger C_{i,E(H),\uparrow(\downarrow)} \rangle$ and $n_{i,\tau} = \sum_\sigma n_{i,\tau,\sigma}$. We note that $\Delta_1 = \Delta_2$ in the absence of a magnetic field.

To understand the physics behind the mean-field results, we first consider the case when the hybridization between the E and H orbitals (t_{EH} and Δ_0) vanishes. In this case, the E and H orbitals form separate bands which overlap because of band inversion (see Fig. 4). A small part of the E band is occupied whereas the H band is almost filled [see Fig. 5(a)]. In this case, the E and H bands are described separately by single-band Hubbard models which are almost empty/filled. Mean-field studies for the single-band Hubbard model on a square lattice were carried out a long time ago [20], and it was found that the ground state is *antiferromagnetic* at and close to half filling and becomes *ferromagnetic* away from half filling when the interaction strength U is larger than a certain critical value. In HgTe/CdTe quantum wells the E and H bands are nearly empty or fully filled at the weak interaction limit, suggesting that we should look for ferromagnetic phases in our mean-field theory. The antiferromagnetic phase is expected only if the band inversion is so large that the two bands are both nearly half filled [the

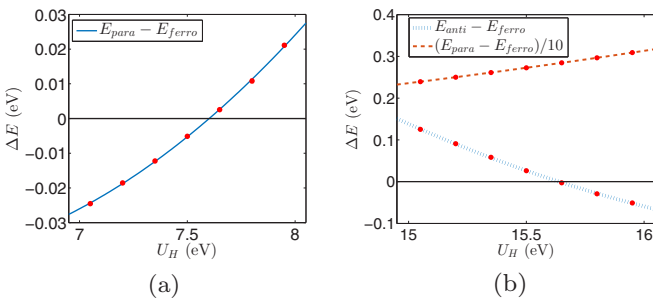


FIG. 5. Energy difference (ΔE) between different phases as a function of U_H with $U_E = 0$, $U_{EH} = 1$ eV. The dots are data calculated self-consistently. (a) Energy difference between *paramagnetic* phase and *ferromagnetic* phase at small $U_H < 10$ eV. There is no *stable antiferromagnetic* phase found in this region. (b) Energy difference between *paramagnetic* phase and *ferromagnetic* phase and energy difference between *antiferromagnetic* phase and *ferromagnetic* phase at large $U_H > 15$ eV. We note that the *antiferromagnetic* phase becomes the ground state only at very large U_H

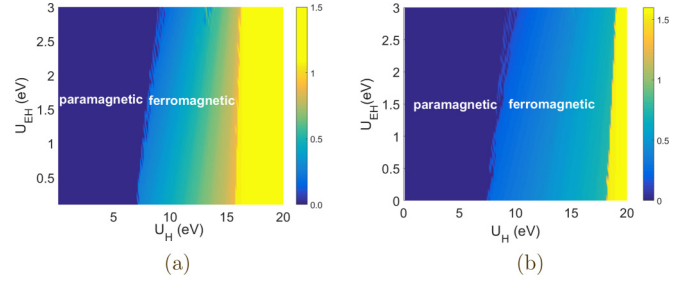


FIG. 6. The mean-field phase diagram as a function of U_H and U_{EH} for (a) $U_E = 0$ and (b) $U_E = 10$ eV. Left region: *paramagnetic* phase; middle region: *ferromagnetic* phase; right region: *antiferromagnetic* phase. The color indicates the magnitude of the magnetic order.

case shown in Fig. 5(b)]. We search for the *paramagnetic*, *ferromagnetic*, and *antiferromagnetic* phases numerically in our study starting from the half filled case for the BHZ model where the chemical potential is in the gap and the system is a topological insulator. We employ the parameters as discussed in the main text, where $t_E = -0.42$ eV, $t_H = 3.32$ eV, $t_{EH} = 0.275$ eV, $\varepsilon_E = 1.67$ eV, $\varepsilon_H = -13.27$ eV [19], and $\Delta_0 = 0.002$ eV. The lattice constant a is chosen to be 1 nm.

We first consider the case with only $U_H \neq 0$, which is similar to the single-band Hubbard model. We note that an important difference between the single-band Hubbard model and the BHZ model is that, in our case, the relative position of the two bands depends on interaction. When U_H increases, the on-site energy of the H orbital is shifted upward while the E orbital energy remains stationary, leading to increasing population in the E band. Changing other interactions has similar effects. Thus we are actually moving along a curve in the density-interaction phase diagram of an effective one-band Hubbard model when interaction changes. For small U_H , only one solution with $m_H = m_E = 0$ is found. As interaction strength increases, two self-consistent solutions appear. The ground state is the one with lower energy. For illustration, we shown the energy difference between different phases as a function of U_H with $U_E = 0$, $U_{EH} = 1$ eV in Fig. 5.

Including U_E and U_{EH} has effects similar to U_H . U_E increases the energy of the E orbital. However, as discussed above, when U_H is weak the occupation number of the E orbital is much smaller than H , and the effect of U_E is much smaller compared to U_H because of the smallness of n_E . Therefore U_E has almost no effect on the phase transition in the weak U_H limit. U_{EH} raises the energies of the two orbital simultaneously but with different values depending on the occupation numbers of the two bands. The shift in the energy of the E (H) orbital is proportional to n_H (n_E). Again, since $n_H \gg n_E$, the energy of the E orbital is shifted faster than the H orbital, leading to decreasing/increasing occupation number in the E/H orbital for $U_{EH} > 0$. The roles of U_E and U_{EH} reverse in the large U_H limit when n_E becomes comparable to n_H .

The dependence of the *paramagnetic-ferromagnetic-antiferromagnetic* phase boundary on the interactions is summarized in the phase diagram in Fig. 6. Comparing the two phase diagrams for $U_E = 0$ and $U_E = 10$ eV, we see that

a large U_E shifts the *paramagnetic-ferromagnetic* boundary only slightly, but it shifts the *ferromagnetic-antiferromagnetic* boundary more significantly, in agreement with our analysis.

APPENDIX C: HYBRIDIZATION BETWEEN LANDAU LEVELS AND EDGE-LIKE STATES

We discuss here how hybridization between electron- and hole-like Landau levels leads to the emergence of the edge-like states. We start with considering the quantum Hall problem using an effective $\mathbf{k} \cdot \mathbf{p}$ Hamiltonian generated from our mean-field Hamiltonian H_{MF} near $\mathbf{k} = 0$ with the effect of the edge simulated by a confining, linear orbital-dependent potential $V_\tau(y)$ (we assume here the edge is along the x direction). For simplicity we neglect the Zeeman energy term and assume $\tilde{\Delta}_1 = \tilde{\Delta}_2 = \Delta$ in our following calculation. The effective Hamiltonian is thus [4]

$$H = \sum_{\mathbf{k}} \tilde{\Psi}_{\mathbf{k}} \mathbf{H}_{k_p}(\mathbf{k}) \Psi_{\mathbf{k}} + \int d^2r V_c(y) \tilde{\Psi}(\mathbf{r}) \Psi(\mathbf{r}), \quad (\text{C1a})$$

where $\Psi(\mathbf{r}) = \{\Psi_{E,\uparrow}(\mathbf{r}), \Psi_{H,\uparrow}(\mathbf{r}), \Psi_{E,\downarrow}(\mathbf{r}), \Psi_{H,\downarrow}(\mathbf{r})\}^T$ and $\Psi_{\mathbf{k}}$ is the Fourier transform of $\Psi(\mathbf{r})$; and

$$\mathbf{H}_{k_p} = -\sigma_0 \tau_0 D k^2 + \sigma_0 \tau_z (M - B k^2 a^2) + \sigma_z \tau_x A k_x - \sigma_0 \tau_y A k_y + \sigma_y \tau_y \Delta, \quad (\text{C1b})$$

where $\sigma_i, \tau_i, i = x, y, z$ are Pauli matrices acting on spin basis and orbit basis respectively. σ_0, τ_0 are the corresponding 2×2 identity matrices, $k^2 = k_x^2 + k_y^2$, $D = (t_E + t_H) a^2 / 2$, $B = (t_E - t_H) a^2 / 2$, $M = \varepsilon_E + 4t_E$, $A = 2t_{EH} a$; and

$$V_\tau(y) = \begin{cases} -\alpha_\tau (y + y_0), & y < -y_0, \\ 0, & -y_0 < y < y_0, \\ \alpha_\tau (y - y_0), & y > y_0 \end{cases} \quad (\text{C1c})$$

is a linear confining potential at the edge which vanishes in the bulk. $\alpha_E > 0$ and $\alpha_H < 0$ for the electron- and hole-like orbitals, respectively. We consider the Landau gauge $\mathbf{A} = -B_z y \hat{x}$ such that H is translational invariant along the x direction and k_x is a good quantum number. In this case, we may replace k_y by $k_y \rightarrow -i\hbar \partial_y - eB_z y$, and H becomes

$$H \rightarrow \begin{pmatrix} K_E & \eta f^\dagger & 0 & -\Delta \\ \eta f & K_H & \Delta & 0 \\ 0 & \Delta & K_E & -\eta f \\ -\Delta & 0 & -\eta f^\dagger & K_H \end{pmatrix}, \quad (\text{C2})$$

where $f = \frac{\xi}{2} + \partial_\xi$, $f^\dagger = \frac{\xi}{2} - \partial_\xi$, $\xi = \sqrt{2}(y - l_B^2 k_x) / l_B$, and $\eta = -\sqrt{2} A / l_B$. $K_\tau = M_\tau + \omega_\tau (f^\dagger f + \frac{1}{2}) + V_\tau(y)$, where $\omega_\tau = -2t_\tau a^2 / l_B^2$ and $M_\tau = \varepsilon_\tau + 4t_\tau$. K_τ is the usual harmonic oscillator type Hamiltonian describing electrons/holes moving in a single orbital and the rest of the terms describe hybridization between different orbitals.

To show how edge-like states emerge, we assume that A and Δ are small compared with Landau level spacings and treat them as perturbations. First we consider $A = 0$, $\Delta = 0$. In this case the eigenvalues and wave functions at the right edge ($k_x l_B^2 > y_0$) are given by

$$\varepsilon_{n,\sigma}^\tau(k_x) = M_\tau + \omega_\tau (n + \frac{1}{2}) + \alpha_\tau (k_x l_B^2 - y_0), \quad (\text{C3})$$

$$\langle \xi | \phi_{n,\tau,\sigma}(k_x) \rangle = \frac{\exp(ik_x x) \exp[-(\xi - \xi'_n)^2 / 2]}{\sqrt{N} \sqrt{2^n n!} \sqrt{\pi}} \times H_n(\xi - \xi'_n) v_{\tau,\sigma}, \quad (\text{C4})$$

where n 's are Landau level indices, H_n is the Hermitian polynomial, $v_{E,\uparrow} = \{1, 0, 0, 0\}^T$, $v_{H,\uparrow} = \{0, 1, 0, 0\}^T$, $v_{E,\downarrow} = \{0, 0, 1, 0\}^T$, and $v_{H,\downarrow} = \{0, 0, 0, 1\}^T$. N is the number of sites in the x direction. The first two terms in $\varepsilon_{n,\sigma}^\tau(k_x)$ describe the bulk LL energy. The last term, which is linear in k_x , is the result of the linear edge potential. Besides the linear dispersion, the linear potential also shifts the wave function guiding center by an amount $\xi'_n = \alpha_\tau \frac{\sqrt{2} l_B^3}{2t_\tau a^2}$ in Eq. (C4).

To determine the value of α_τ , we notice that the linear potential gives rise to a drift velocity $v_{d,\tau} = \alpha_\tau l_B^2 / \hbar$ along the edge. The slope α_τ can be determined by comparing this drift velocity with the drift velocity computed for IQH states with a sharp edge, where the semi-classical picture gives $v_{d,\tau} = 2/\pi \sqrt{\omega_\tau (n + 1/2) / m_\tau^*}$. $m_\tau^* \approx -\hbar^2 / (t_\tau a^2)$ is the effective mass of τ orbital near the band edge. Comparing the two results, we find that $\alpha_\tau \sim -\frac{t_\tau a^2}{l_B^3}$. Substituting into ξ'_n we find that the wave function shift depends on the LL index only, with $\xi'_n = 2\sqrt{2}/\pi \sqrt{n + 1/2}$.

When A and Δ are turned on, A couples in the bulk $|\phi_{1,E,\uparrow}(k_x)\rangle$ with $|\phi_{0,H,\uparrow}(k_x)\rangle$ and $|\phi_{0,E,\downarrow}(k_x)\rangle$ with $|\phi_{1,H,\downarrow}(k_x)\rangle$. What is interesting is that the $n = 0$ electron and hole levels $|\phi_{0,E,\sigma}(k_x)\rangle$ and $|\phi_{0,H,\sigma}(k_x)\rangle$ are also coupled at the edge due to the shift in the guiding center of the wave functions. With this in mind we write down an effective Hamiltonian for the $n = 0$ LLs. In the basis $\{|\phi_{0,E,\uparrow}(k_x)\rangle, |\phi_{0,H,\uparrow}(k_x)\rangle, |\phi_{0,E,\downarrow}(k_x)\rangle, |\phi_{0,H,\downarrow}(k_x)\rangle\}^T$, the effective Hamiltonian becomes

$$H_0 = \begin{pmatrix} H_{0,\uparrow} & H_\Delta \\ H_\Delta^\dagger & H_{0,\downarrow} \end{pmatrix}, \quad H_{0,\sigma} = \begin{pmatrix} \varepsilon_{0,\sigma}^E & s\eta h_0 \\ s\eta h_0 & \varepsilon_{0,\sigma}^H \end{pmatrix}, \quad H_\Delta = \begin{pmatrix} 0 & -\Delta \\ \Delta & 0 \end{pmatrix}, \quad (\text{C5})$$

where $s = +(-)1$ for $\sigma = \uparrow (\downarrow)$ and

$$h_0 = \langle \phi_{0,E,\uparrow}(k_x) | f^\dagger \sigma_z \tau_x | \phi_{0,H,\uparrow}(k_x) \rangle \\ = \langle \phi_{0,E,\uparrow}(k_x) | \frac{\xi - \xi'_0}{2} - \partial_{\xi - \xi'_0} + \xi'_0 / 2 | \phi_{0,E,\uparrow}(k_x) \rangle \\ = \xi'_0 / 2 \quad (\text{C6})$$

is the matrix element describing the (same spin) electron-hole hybridization. $\sigma_z \tau_x$ is the operator that flips the orbital index. h_0 vanishes in the bulk and is nonzero only in the edge due to the shift in the wave function guiding center by the linear potential, as illustrated above. It is straightforward to diagonalize H_0 to obtain the eigen-energies

$$\varepsilon_{p,\pm}(k_x) = \frac{\varepsilon_{0,\uparrow}^E(k_x) + \varepsilon_{0,\downarrow}^H(k_x)}{2} \pm \varepsilon_{p,0}(k_x), \quad (\text{C7a})$$

where

$$\varepsilon_{p,0}(k_x) = \sqrt{\left(\frac{\varepsilon_{0,\uparrow}^E(k_x) - \varepsilon_{0,\downarrow}^H(k_x)}{2} \right)^2 + (\Delta + \eta \xi'_0 / 2)^2} \quad (\text{C7b})$$

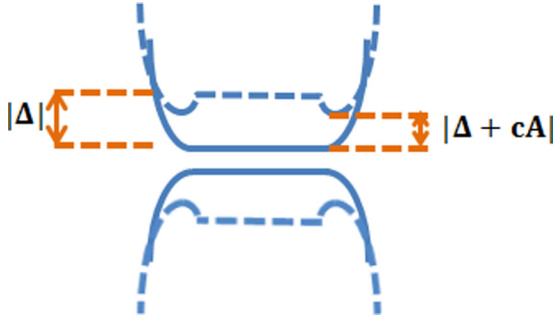


FIG. 7. Schematic band structure to illustrate the emergence of the edge-like state for the zeroth LL. Without the BIA term, the zeroth LL has same spin electron-hole hybridization only at the edge (solid line) arising from A term $\sim t_{EH}$. When BIA term is turned on, it opens a hybridization gap (dashed line) at the bulk while the effective hybridization $\sim |\Delta + cA|$ is weakened at the edge.

and

$$\varepsilon_{m,\pm}(k_x) = \frac{\varepsilon_{0,\downarrow}^E(k_x) + \varepsilon_{0,\uparrow}^H(k_x)}{2} \pm \varepsilon_{m,0}(k_x), \quad (C7c)$$

where

$$\varepsilon_{m,0}(k_x) = \sqrt{\left(\frac{\varepsilon_{0,\downarrow}^E(k_x) - \varepsilon_{0,\uparrow}^H(k_x)}{2}\right)^2 + (\Delta - \eta\xi'_0/2)^2}. \quad (C7d)$$

The first term under the square root is the unperturbed LL spacing. The second term, $(\Delta \pm \eta\xi'_0/2)^2$, is the hybridization contributed by A and Δ . The low energy sector is described by $\varepsilon_{p,\pm}$ since $\eta < 0$ from our band parameters. We notice that

the hybridization term $(\Delta + \eta\xi'_0/2)$ at the edge is smaller than that of in the bulk ($\sim \Delta$) as long as $\Delta > -\eta\xi'_0/4$. This effect exists only when both $\eta \sim A$ and Δ are nonzero. This physical picture is illustrated in Fig. 7.

As a result, it is possible that $\varepsilon_{p,+(-)}(k_x)$ at the edge ($|k_x|l_B^2 > y_0$) are smaller than their values in bulk ($|k_x|l_B^2 < y_0$). Assuming $\Delta_0 + \eta\xi'_0/2 \ll [\varepsilon_{0,\uparrow}^E(k_x) - \varepsilon_{0,\downarrow}^H(k_x)]/2$, we obtain

$$\varepsilon_{p,+(-)}(|k_x| < y_0) \sim \omega_{E(H)} \pm \frac{\Delta^2}{\omega_E - \omega_H}$$

and

$$\varepsilon_{p,+(-)}(|k_x| > y_0) \sim \omega_{E(H)} + \alpha_{E(H)}(|k_x|l_B^2 - y_0) \quad (C8)$$

$$\pm \frac{(\Delta + \eta\xi'_0/2)^2}{\omega_E - \omega_H + (\alpha_E - \alpha_H)(|k_x|l_B^2 - y_0)}. \quad (C9)$$

We have neglected M_τ since its not important beyond critical magnetic field B_c defined in main text. It is easy to see that there exists a finite region $y_0 < k_x l_B^2 < k_c l_B^2$ where $\varepsilon_{p,+(-)}(|k_x|l_B^2 < y_0) > \varepsilon_{p,+(-)}(|k_x|l_B^2 > y_0)$.

By keeping terms up to first order in $k_x l_B^2 - y_0$, k_c is given by

$$\Delta^\tau + \frac{\xi'_0 \eta}{4} \approx - \frac{2(t_H - t_E)|t_\tau|a^4(k_c l_B^2 - y_0)}{\eta\xi'_0 l_B^5}. \quad (C10)$$

We note that k_c depends on the magnitude of hopping t_τ . When $|t_E| < |t_H|$, corresponding to $D > 0$, $k_c^E > k_c^H$ and the nontopological edge state is easier to observe in the electron-like LL, consistent with the experimental result. Therefore, we chose $D > 0$ for the calculation in the main text.

-
- [1] B. A. Bernevig, T. L. Hughes, and S. C. Zhang, *Science* **314**, 1757 (2006).
- [2] I. Knez and R. R. Du, *Front. Phys.* **7**, 200 (2012).
- [3] M. Z. Hasan and C. L. Kane, *Rev. Mod. Phys.* **82**, 3045 (2010).
- [4] X. L. Qi and S. C. Zhang, *Rev. Mod. Phys.* **83**, 1057 (2011).
- [5] D. G. Rothe, R. W. Reinthaler, C.-X. Liu, L. W. Molenkamp, S.-C. Zhang, and E. M. Hankiewicz, *New J. Phys.* **12**, 065012 (2010).
- [6] M. König, H. Buhmann, L. W. Molenkamp, T. Hughes, C. X. Liu, X. L. Qi, and S. C. Zhang, *J. Phys. Soc. Jpn.* **77**, 031007 (2008).
- [7] M. König, S. Wiedmann, C. Brüne, A. Roth, H. Buhmann, L. W. Molenkamp, X. L. Qi, and S. C. Zhang, *Science* **318**, 766 (2007).
- [8] B. Buttner, C. X. Liu, G. Tkachov, E. G. Novik, C. Brüne, H. Buhmann, E. M. Hankiewicz, P. Recher, B. Trauzette, S. C. Zhang, and L. W. Molenkamp, *Nat. Phys.* **7**, 418 (2011).
- [9] C. Brüne, A. Roth, H. Buhmann, E. M. Hankiewicz, L. W. Molenkamp, J. Maciejko, X. L. Qi, and S. C. Zhang, *Nat. Phys.* **8**, 485 (2012).
- [10] L. Fu and C. L. Kane, *Phys. Rev. B* **76**, 045302 (2007).
- [11] B. Scharf, A. Matos-Abiague, and J. Fabian, *Phys. Rev. B* **86**, 075418 (2012).
- [12] J.-c. Chen, J. Wang, and Q.-f. Sun, *Phys. Rev. B* **85**, 125401 (2012).
- [13] G. Tkachov and E. M. Hankiewicz, *Phys. Rev. Lett.* **104**, 166803 (2010).
- [14] M. Orlita, K. Masztalerz, C. Faugeras, M. Potemski, E. G. Novik, C. Brüne, H. Buhmann, and L. W. Molenkamp, *Phys. Rev. B* **83**, 115307 (2011).
- [15] M. Zholudev, F. Tepe, M. Orlita, C. Consejo, J. Torres, N. Dyakonova, M. Czapkiewicz, J. Wrobel, G. Grabecki, N. Mikhailov, S. Dvoretzkii, A. Ikonnikov, K. Spirin, V. Aleshkin, V. Gavrilenko, and W. Knap, *Phys. Rev. B* **86**, 205420 (2012).
- [16] L. Du, I. Knez, G. Sullivan, and R. R. Du, *Phys. Rev. Lett.* **114**, 096802 (2015).
- [17] S. B. Zhang, Y. Y. Zhang, and S. Q. Shen, *Phys. Rev. B* **90**, 115305 (2014).
- [18] E. Y. Ma, M. R. Calvo, J. Wang, B. Lian, M. Mühlbauer, C. Brüne, Y. T. Cui, K. Lai, W. Kundhikanjana, Y. Yang *et al.*, *Nat. Commun.* **6**, 7252 (2015).
- [19] W. Beugeling, C. X. Liu, E. G. Novik, L. W. Molenkamp, and C. Morais Smith, *Phys. Rev. B* **85**, 195304 (2012).
- [20] J. E. Hirsch, *Phys. Rev. B* **31**, 4403 (1985).